Supporting information

A Highly Selective Chemosensor for Cyanide Derived from a Formyl Functionalized Phosphorescent Iridium(III) Complex

K. S. Bejoymohandas,[§,†,¶] *Ajay Kumar,*[§,¶] *S. Sreenadh,*[§] *E. Varathan,*[‡], *S. Varughese,*[§] *V. Subramanian,*[‡] *and M. L. P. Reddy**[,§,†]

[§]Materials Science and Technology Division, CSIR-Network of Institutes for Solar Energy, CSIR-National Institute for Interdisciplinary Science & Technology (CSIR-NIIST), Thiruvananthapuram-695 019, India

[†]Academy of Scientific and Innovative Research (AcSIR), New Delhi 110025, India.

[‡]Chemical Laboratory, CSIR-Central Leather Research Institute, Chennai – 600 020, India

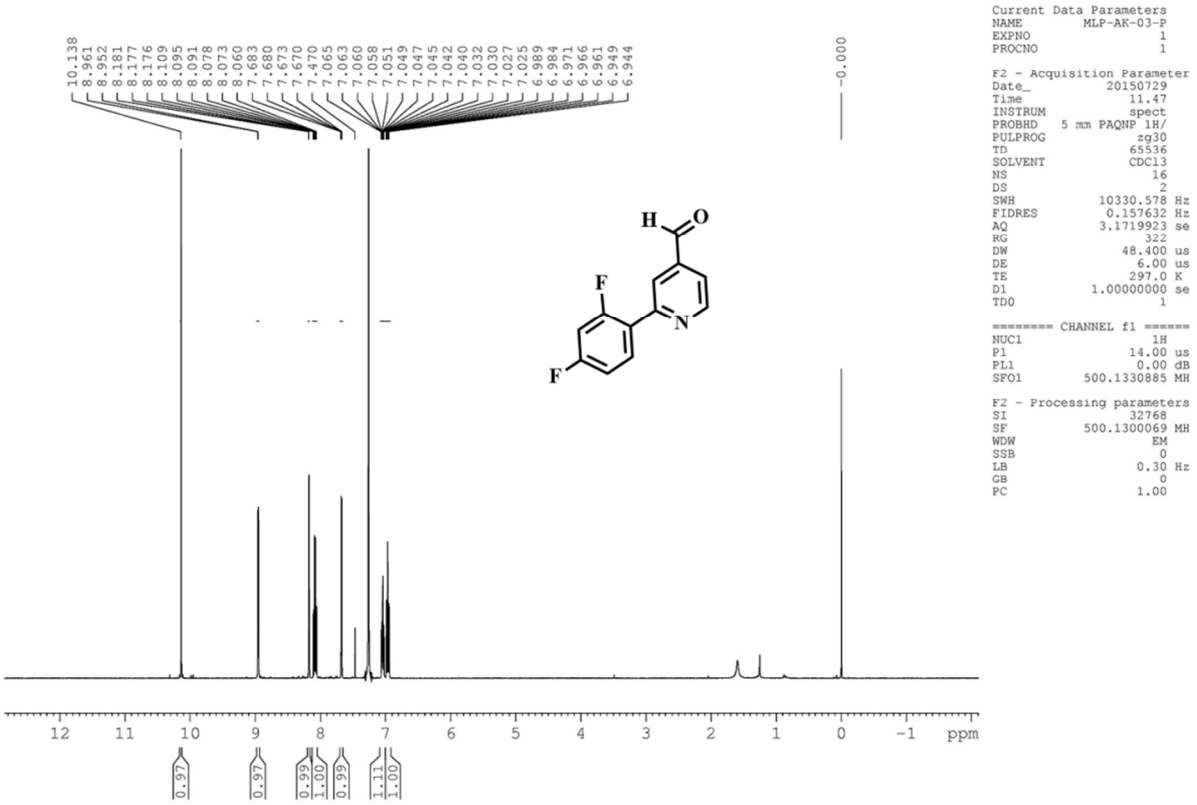

Figure S1. ^{1}H-NMR spectrum of 2',6'-difluorophenyl-4-(formyl)pyridine.

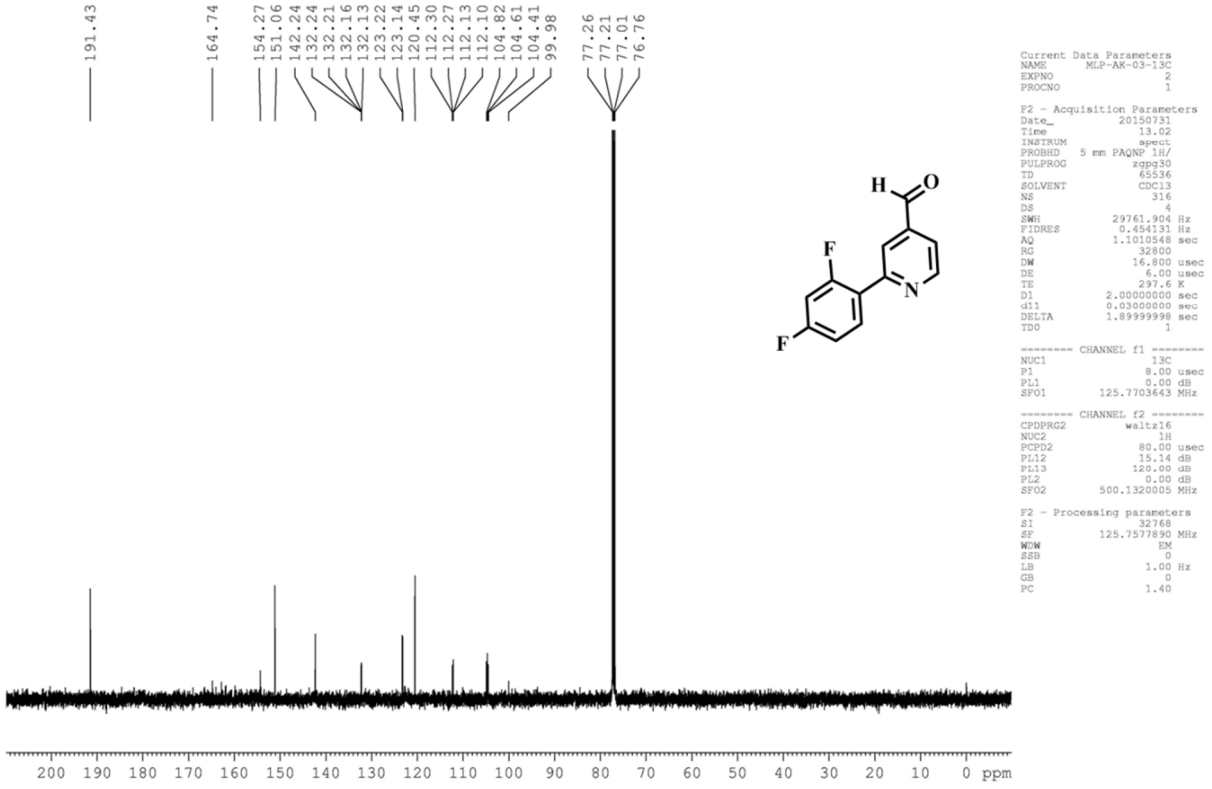

Figure S2. ^{13}C-NMR spectrum of 2',6'-difluorophenyl-4-(formyl)pyridine.

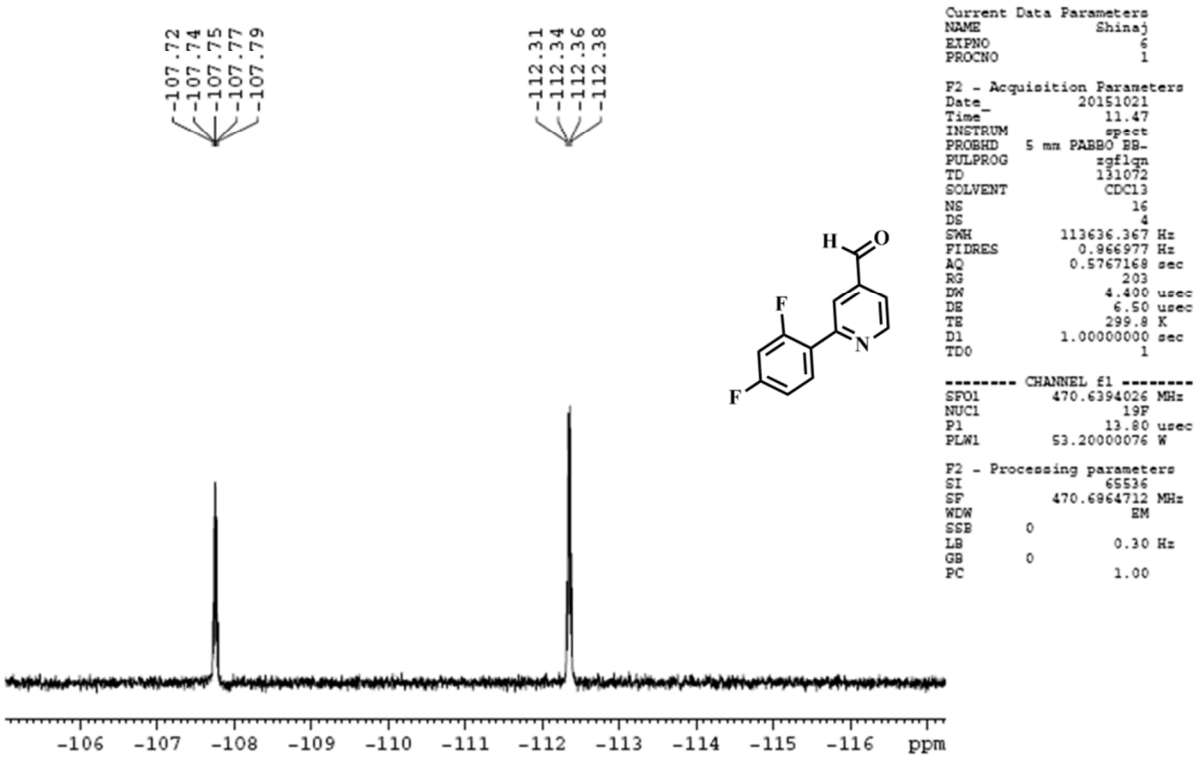

Figure S3 ^{19}F-NMR spectrum of 2',6'-difluorophenyl-4-(formyl)pyridine.

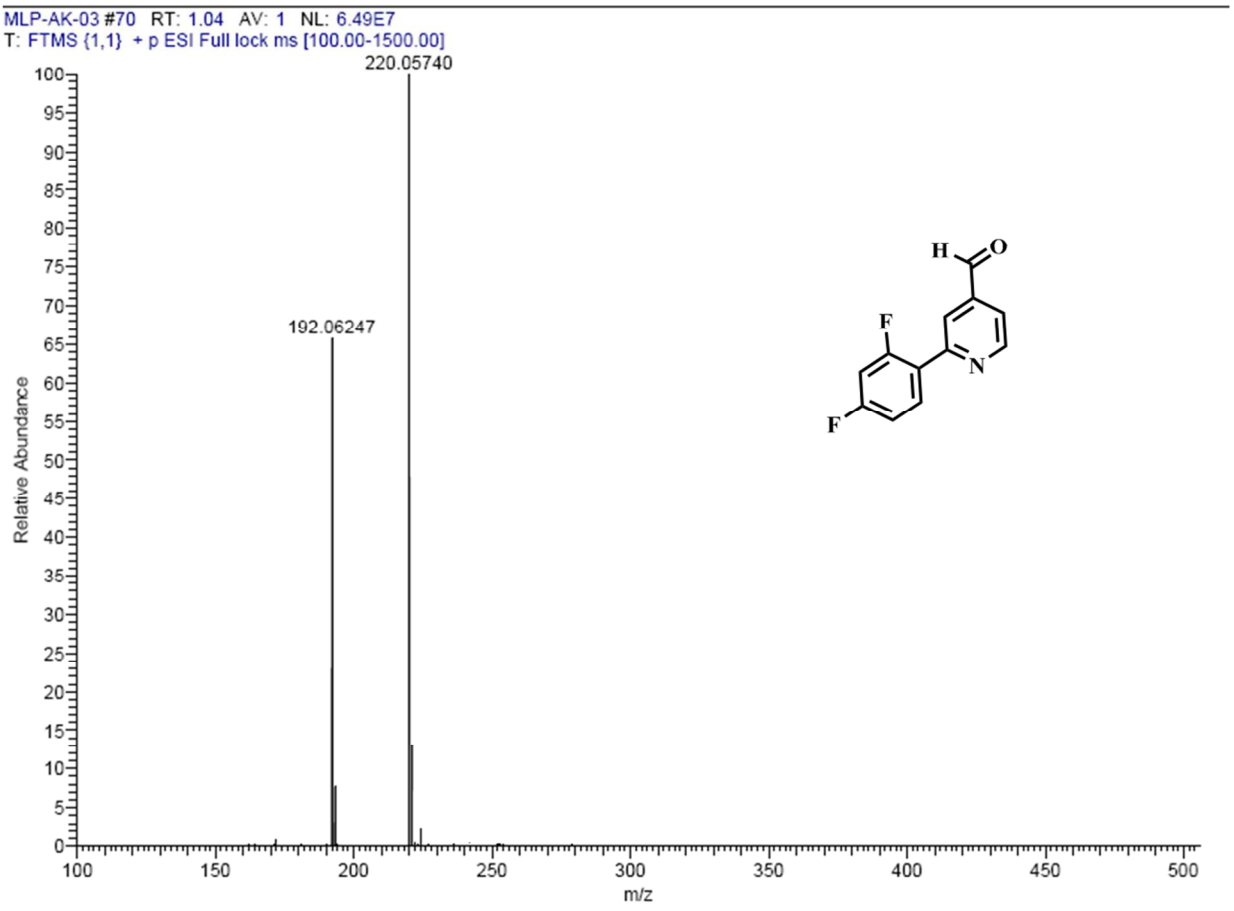

Figure S4. ESI-MS spectrum of 2',6'-difluorophenyl-4-(formyl)pyridine, 220.05(M+1).

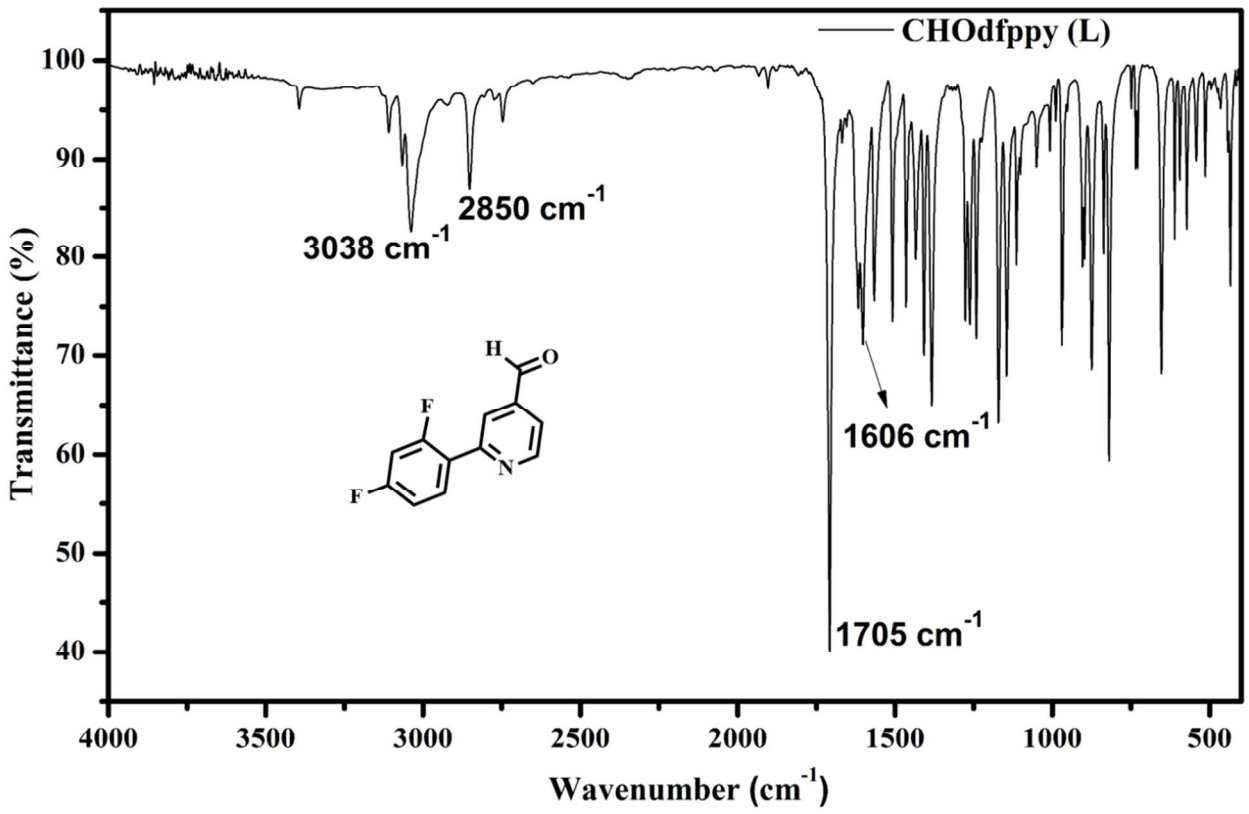

Figure S5. FT-IR spectrum of 2',6'-difluorophenyl-4-(formyl)pyridine.

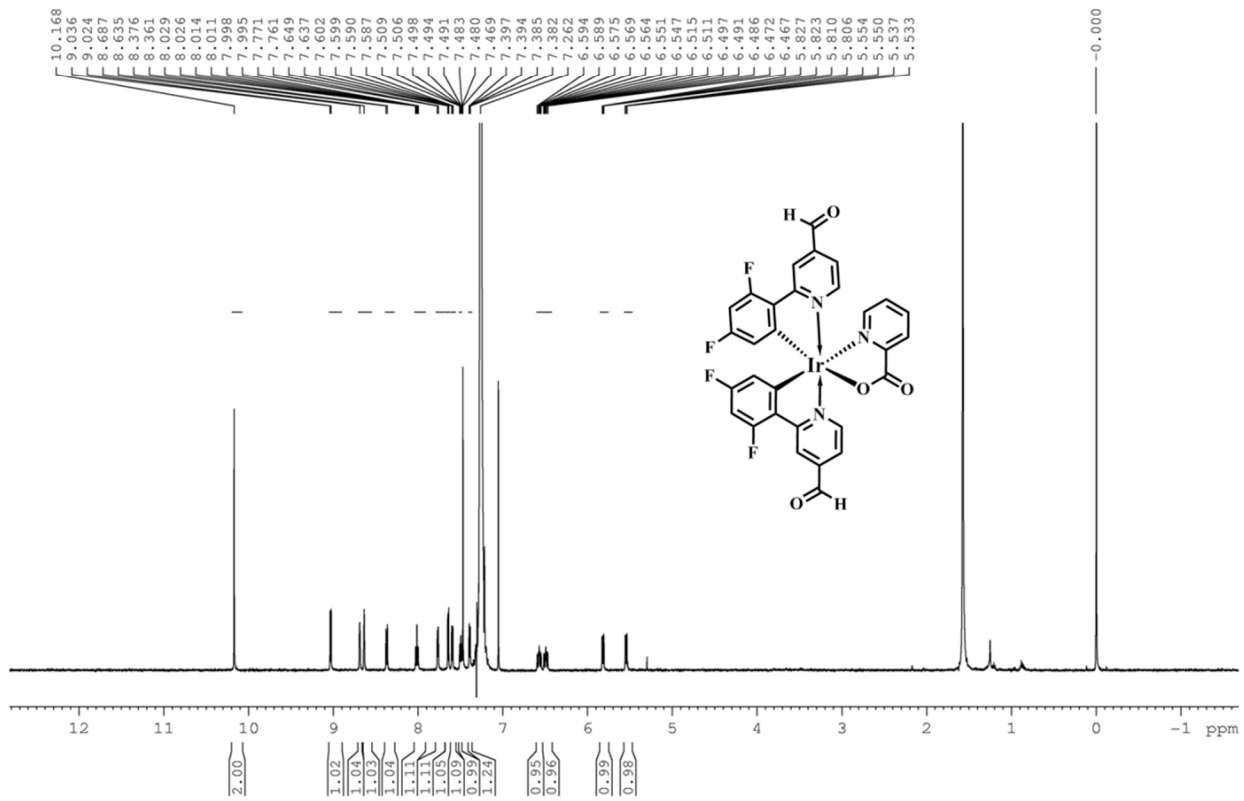

Figure S6. ^{1}H-NMR spectrum of bis[2',6'-difluorophenyl-4-formylpyridinato-N,C4′]iridium(III) (picolinate).

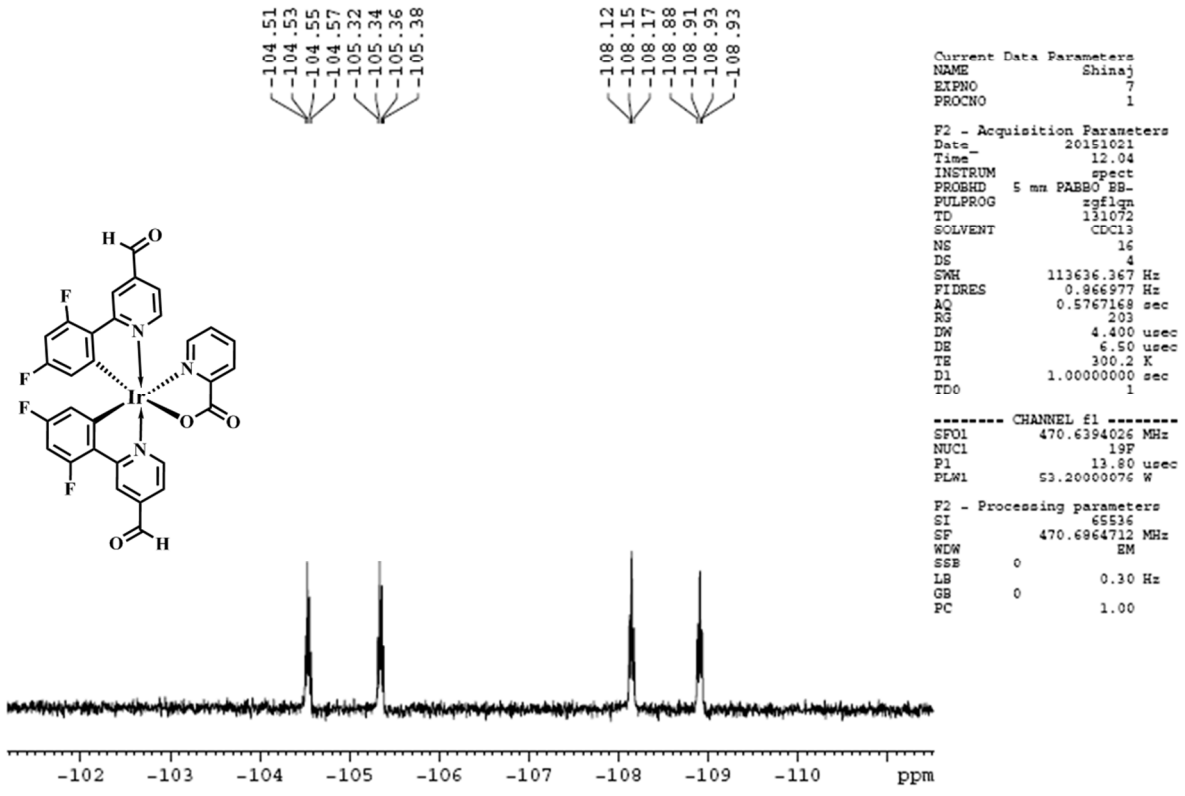

Figure S7. ^{19}F-NMR spectrum of bis[2',6'-difluorophenyl-4-formylpyridinato-N,C4′]iridium(III) (picolinate).

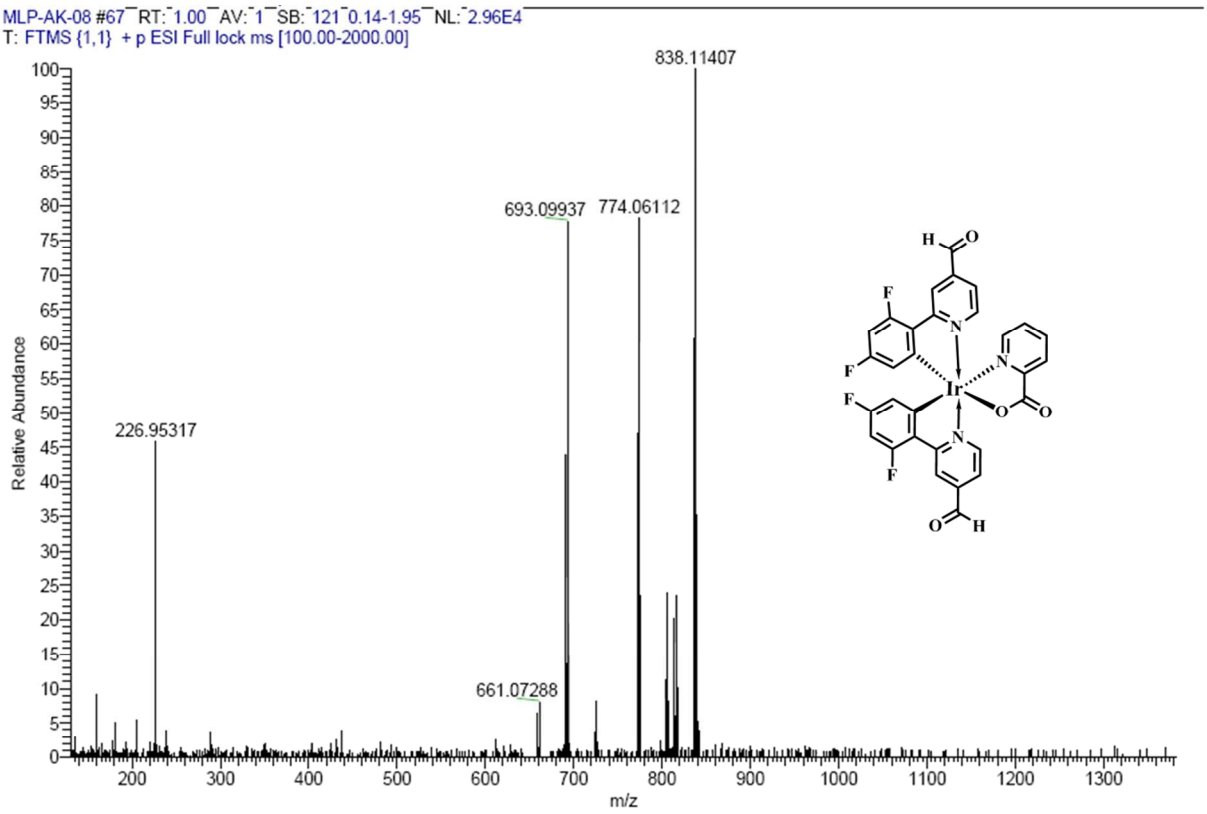

Figure S8. ESI-MS spectrum of bis[2',6'-difluorophenyl-4-formylpyridinato-N,C4′]iridium(III) (picolinate). **IrC**+ Na: m/z = 774.06 [M+1], **IrC**+ $2CH_3OH$+ Na: m/z = 838.11. [M+1].

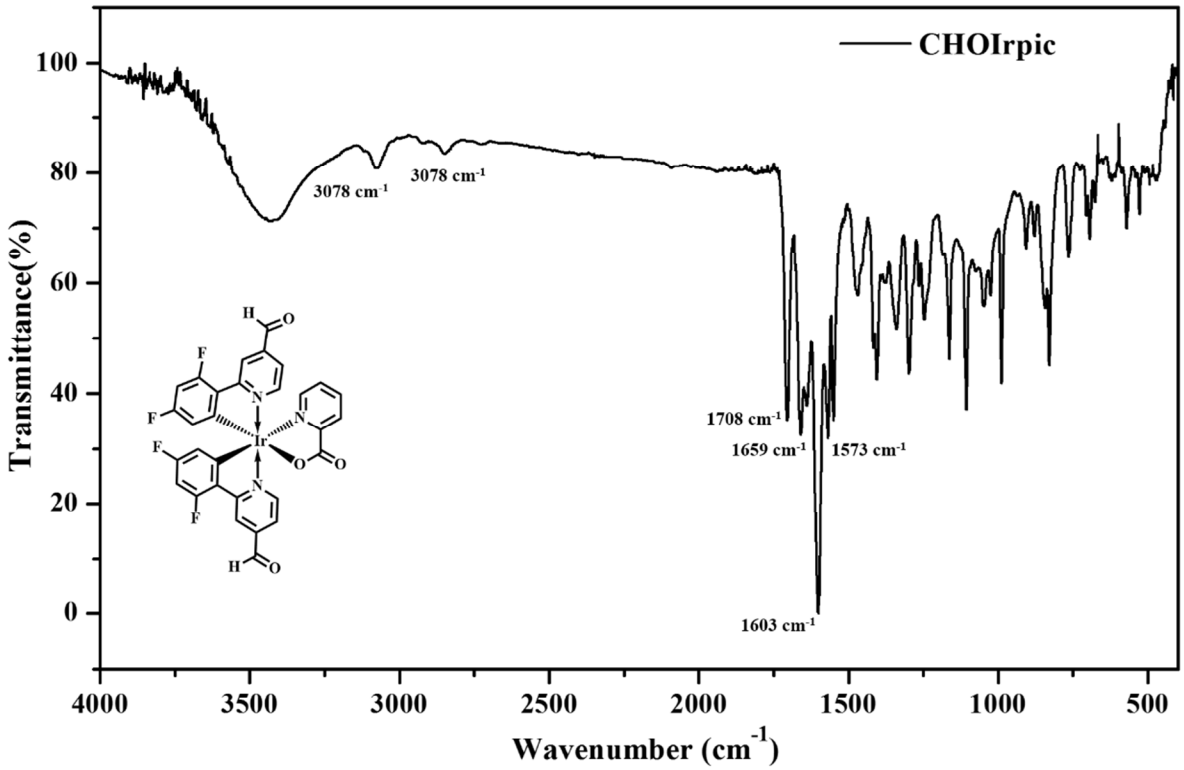

Figure S9. FT-IR spectrum of bis[2',6'-difluorophenyl-4-formylpyridinato-N,C4′]iridium(III) (picolinate).

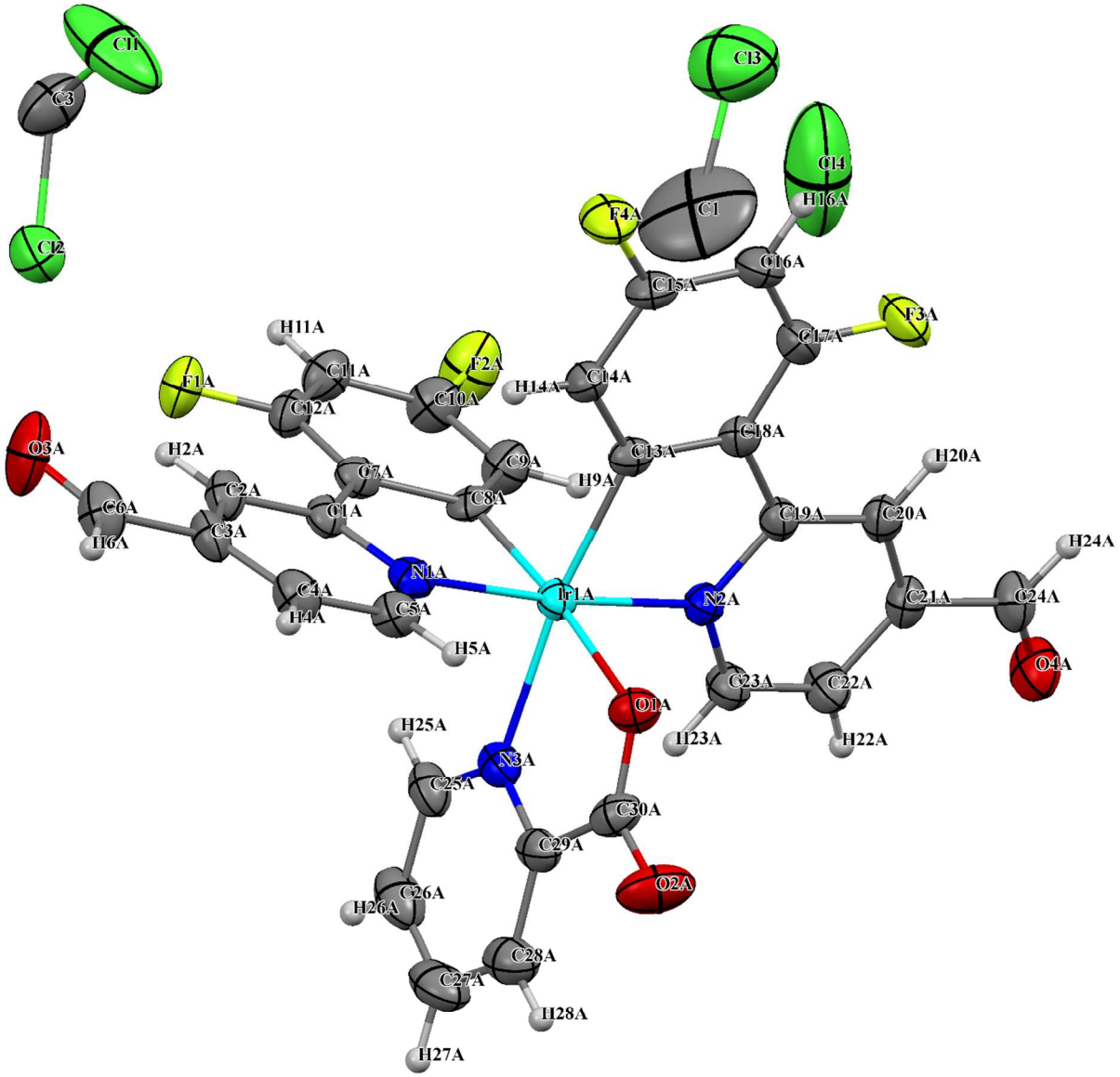

Figure S10. X-Ray single crystal structure of the complex **IrC** with complete atom numbering. Thermal ellipsoid drawing is presented at the 30% probability level.

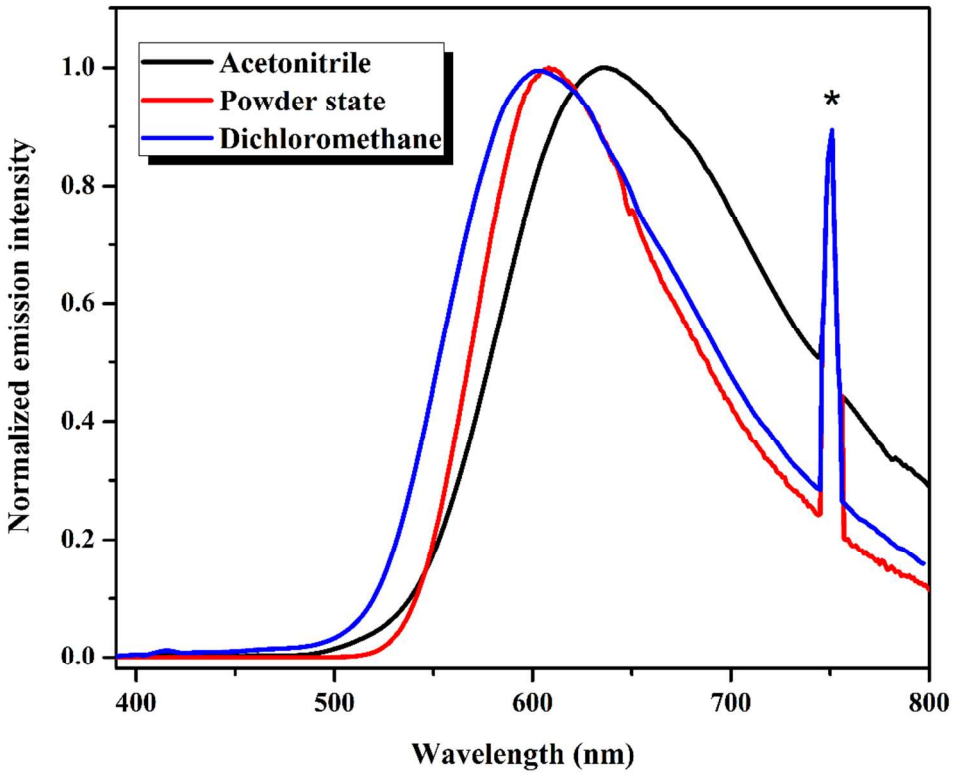

Figure S11. Comparison of normalized emission profiles of **IrC** recorded in acetonitrile, dichloromethane and powder state at 298 K (λ_{exc} = 375 nm).

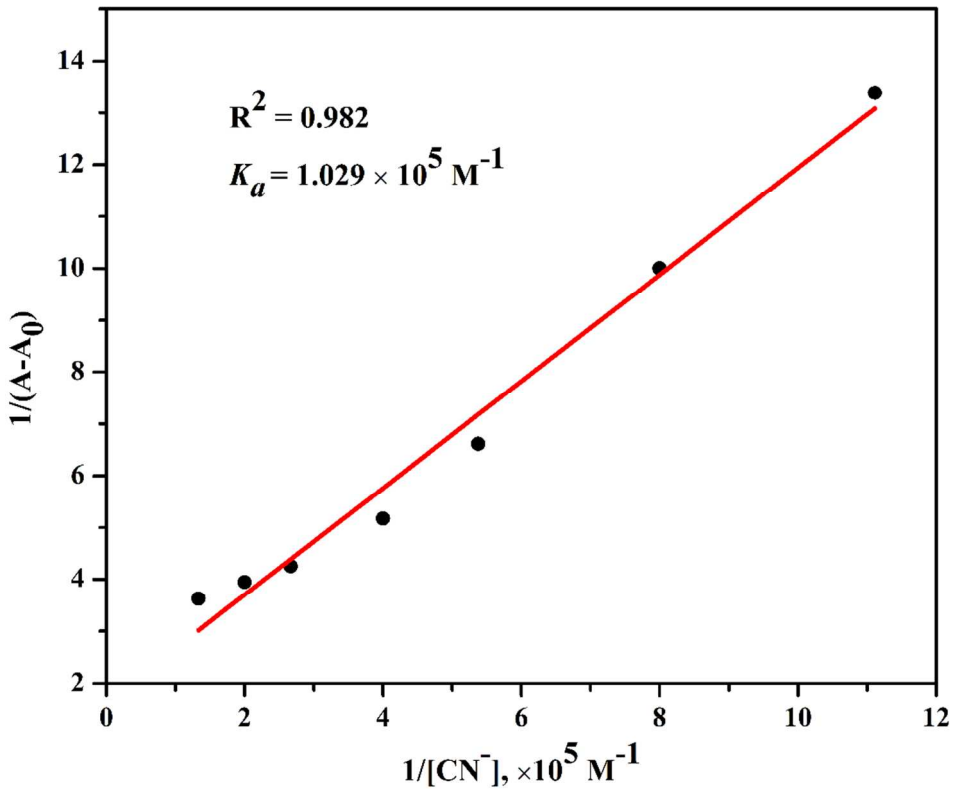

Figure S12. Benesi-Hildebrand plot of **IrC** with CN^-.

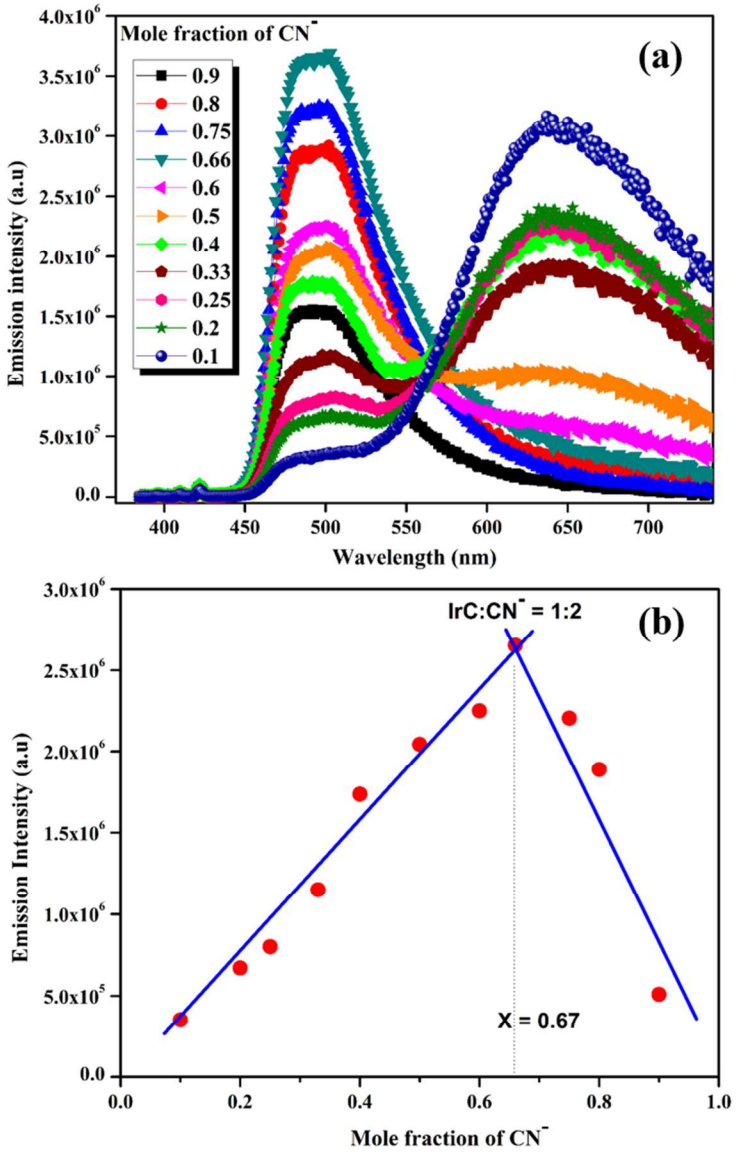

Figure S13. (a) Phosphorescence emission spectra of **IrC+(CN^-)** adduct complexes at different mole fractions of CN^- in CH_3CN at 298K (λ_{exc}= 375 nm) **(b)** Job plot of **IrC+(CN^-)** adduct complexes, where the phosphorescence emission intensity at 480 nm is plotted against mole fraction of CN^-, at a constant total concentration of 2.0×10^{-5} M in acetonitrile solutions.

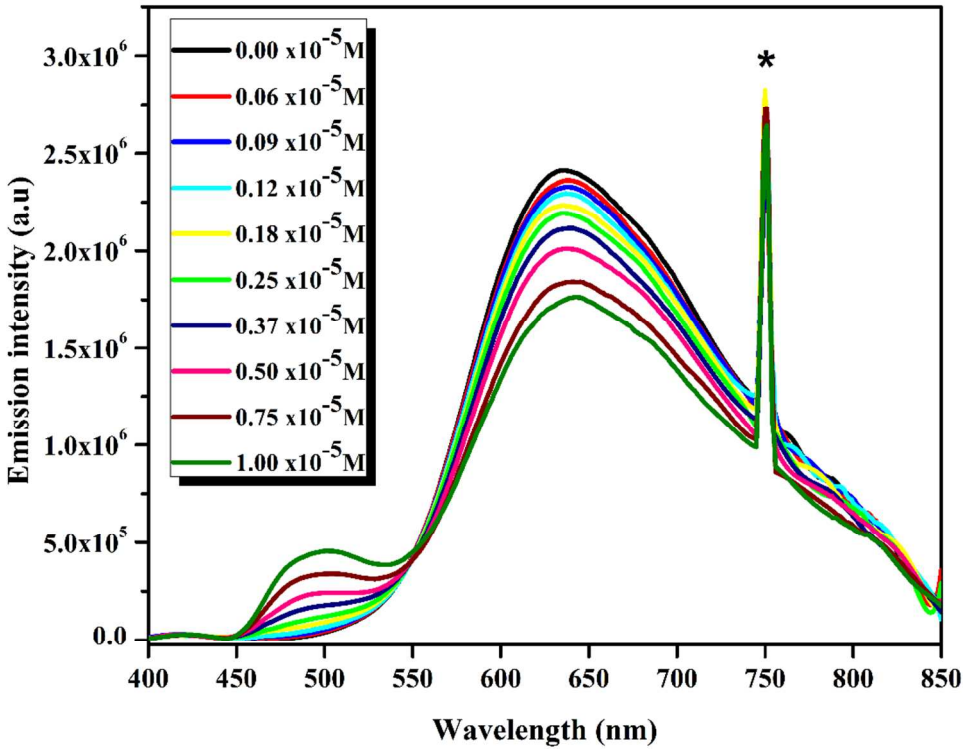

Figure S14. Photoluminescence titration of **IrC** with low concentration levels of CN^-**)** (0.0-10.0 μM) (λ_{exc} = 375 nm). At 750 nm (*) indicates the second harmonic peak of the excitation wavelength.

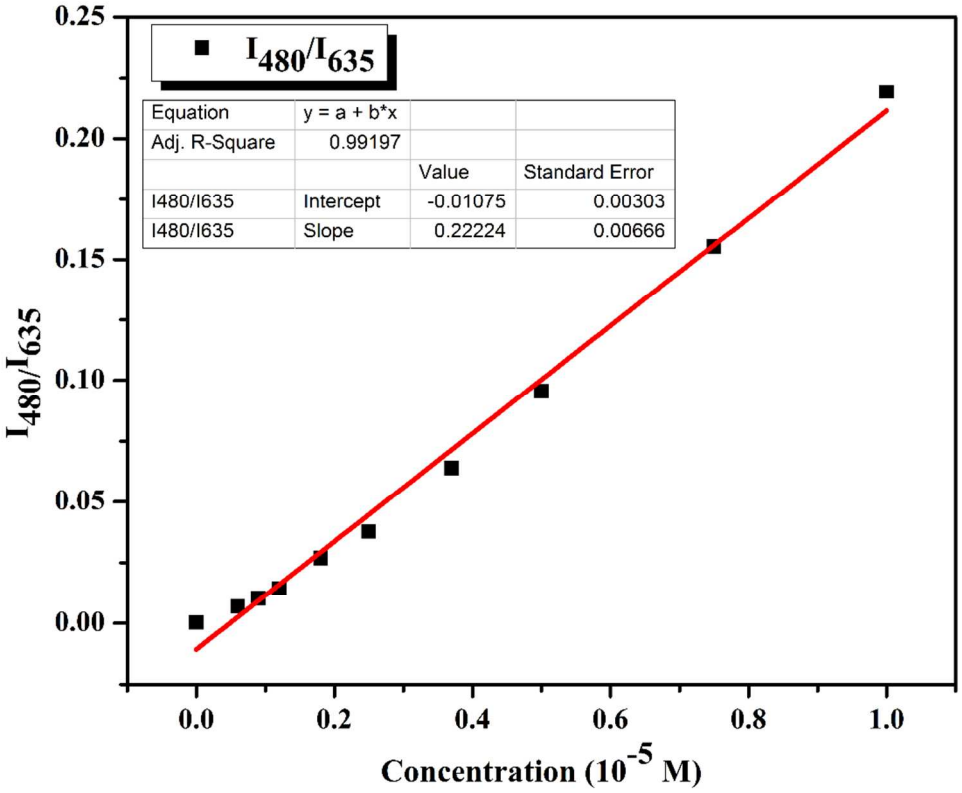

Figure S15. Plot of I_{480}/I_{635} *vs* CN^- (0.0-10.0 μM) shows a good linear relationship.

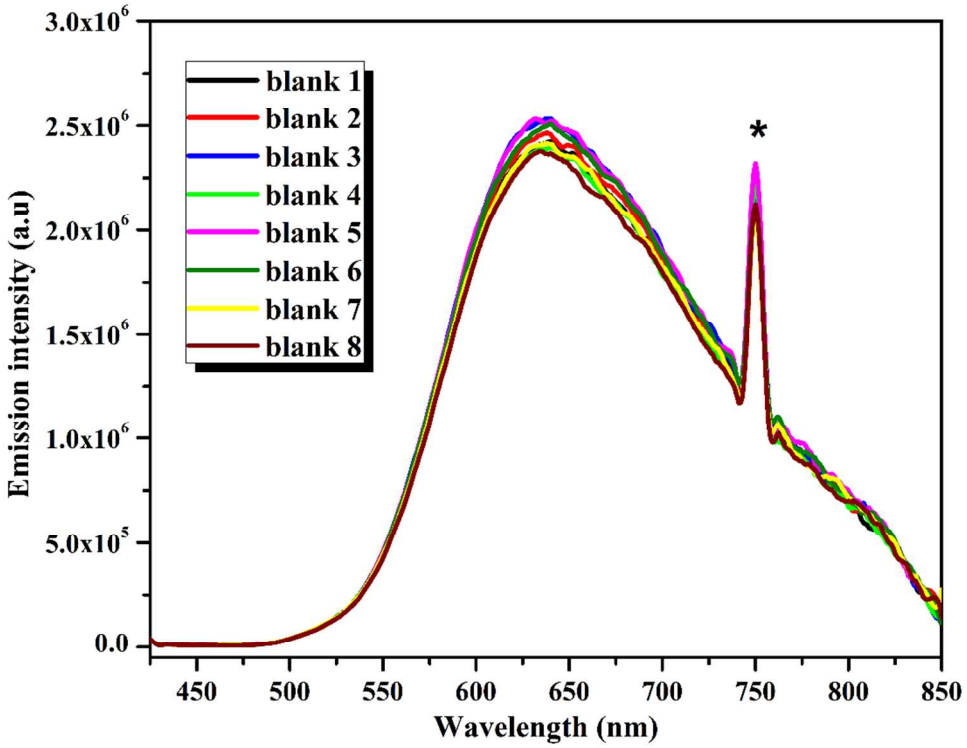

Figure S16. Photoluminescence of **IrC** (20.0 μM) solutions for the calculation of standard deviation before the CN^- titration experiment (λ_{exc}= 375 nm). At 750 nm (*) indicates the second harmonic peak of the excitation wavelength.

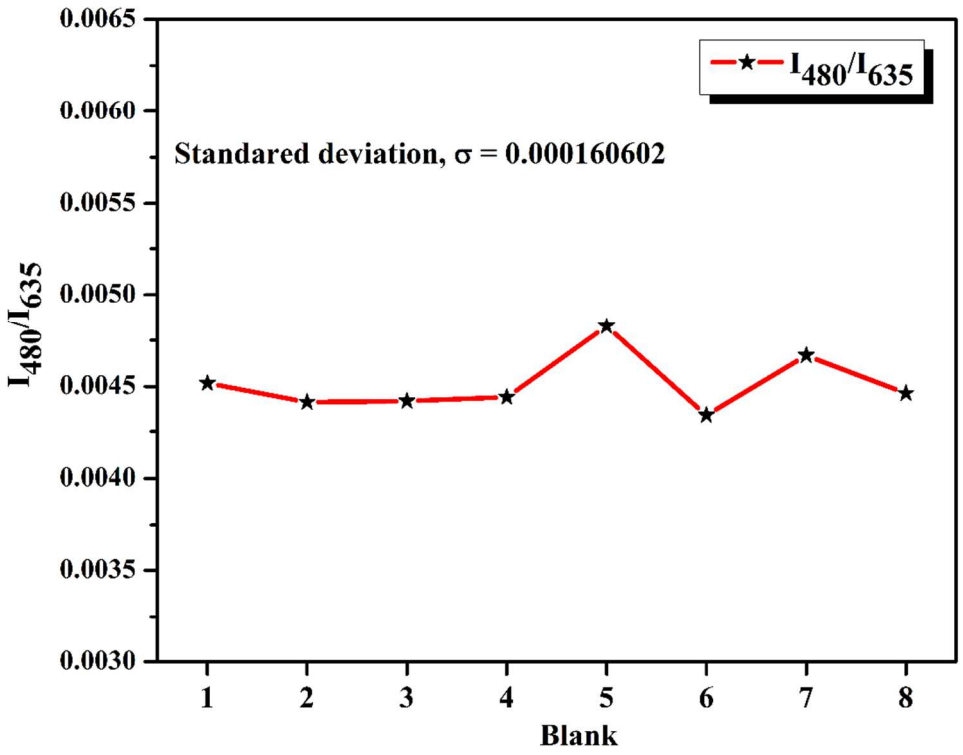

Figure S17. Plot of I_{480}/I_{635} vs blank solutions for the calculation of standard deviation.

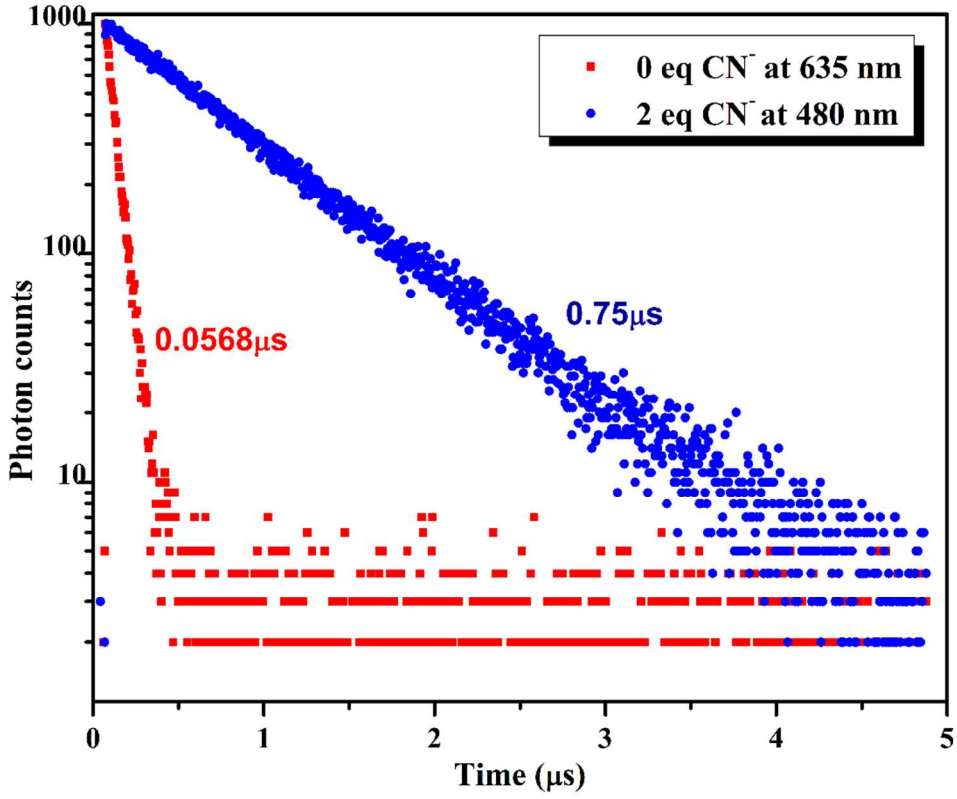

Figure S18. Lifetime decay profiles of **IrC** (c = 20 μM) in acetonitrile at 635 nm before adding CN^- and at 480 nm after adding 2.0 equiv of CN^- (λ_{exc}= 375 nm).

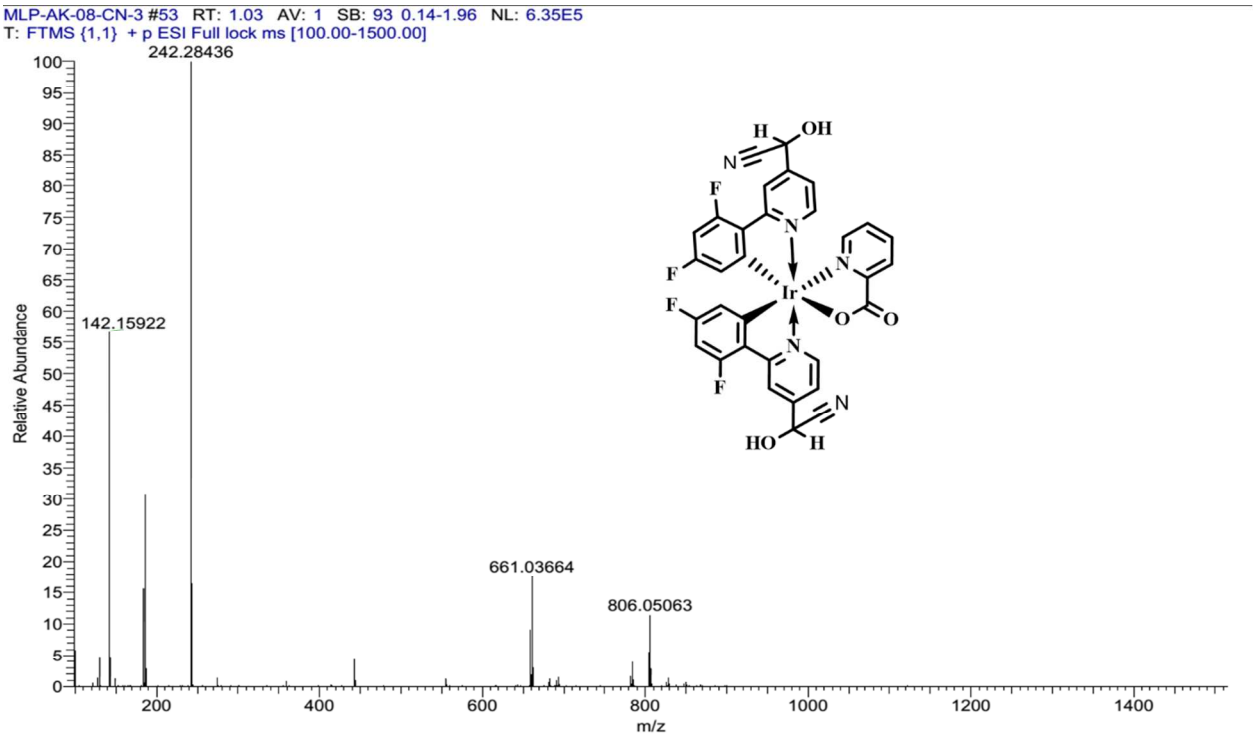

Figure S19. ESI-MS spectrum of (2',6'-difluoro-4-(formyl)-2,3'-bipyridinato-N,C4′) Iridium(III) (picolinate), [**IrC**] after addition of 2.0 equivalents of CN^- anions. **IrC+(CN)$_2$**: m/z = 806.05 [M^{+1}].

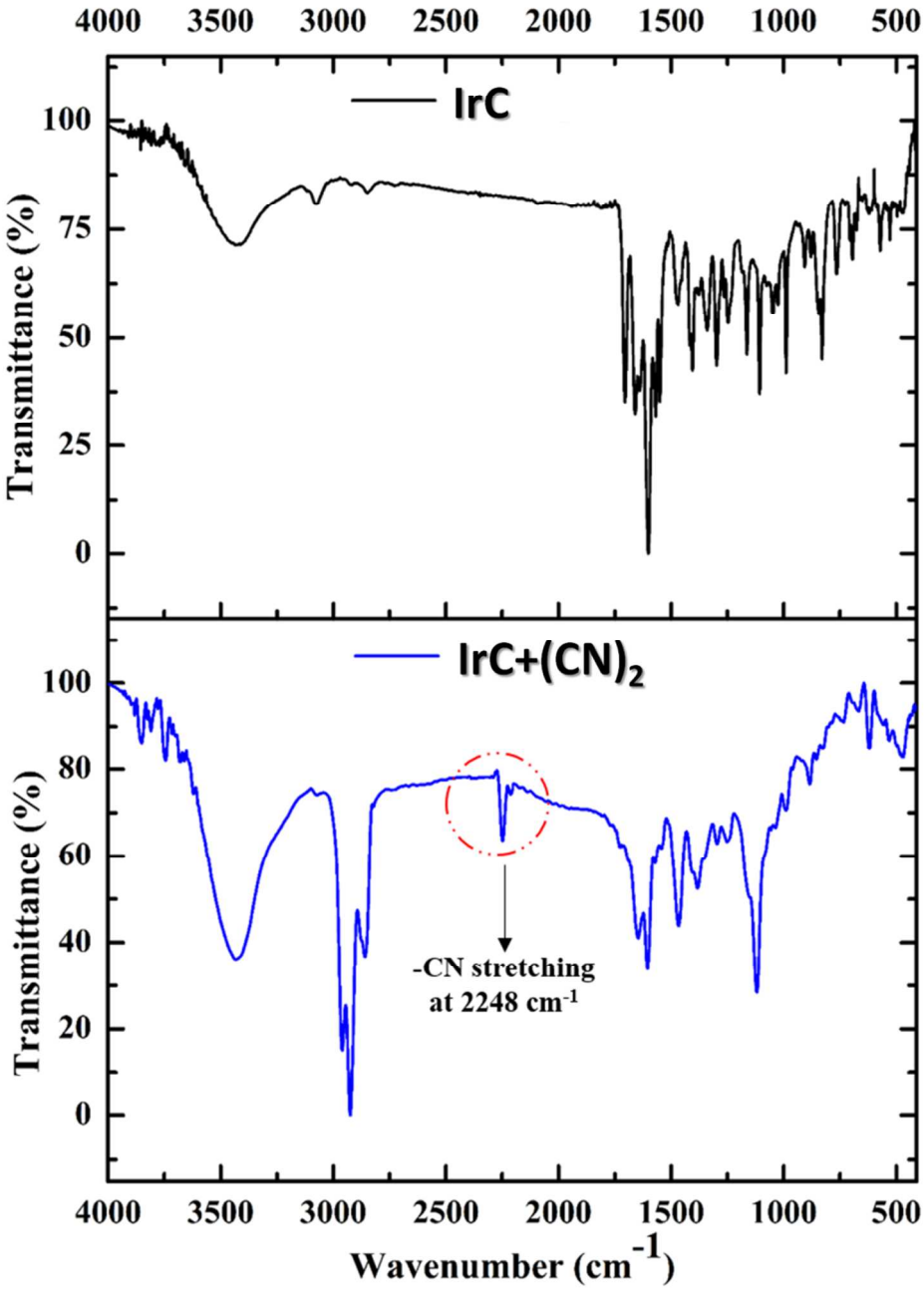

Figure S20. Comparison of FT-IR spectrum of **IrC** before and after the addition of 2.0 equiv of CN^- anion.

Table S1. Complete list of bond angles in IrC

Number	Atom1	Atom2	Atom3	Angle(°)	Number	Atom1	Atom2	Atom3	Angle(°)
1	O1A	Ir1A	N1A	95.0(2)	36	C3A	C4A	C5A	119.6(7)
2	O1A	Ir1A	N2A	88.8(2)	37	H4A	C4A	C5A	120.1(8)
3	O1A	Ir1A	N3A	76.8(2)	38	N1A	C5A	C4A	122.4(7)
4	O1A	Ir1A	C8A	174.7(3)	39	N1A	C5A	H5A	118.8(7)
5	O1A	Ir1A	C13A	95.4(3)	40	C4A	C5A	H5A	118.8(8)
6	N1A	Ir1A	N2A	174.2(2)	41	O3A	C6A	C3A	124.4(9)
7	N1A	Ir1A	N3A	89.6(2)	42	C1A	C7A	C8A	115.5(6)
8	N1A	Ir1A	C8A	80.6(3)	43	C1A	C7A	C12A	125.9(7)
9	N1A	Ir1A	C13A	94.8(3)	44	C8A	C7A	C12A	118.5(7)
10	N2A	Ir1A	N3A	95.5(3)	45	Ir1A	C8A	C7A	114.1(5)
11	N2A	Ir1A	C8A	95.9(3)	46	Ir1A	C8A	C9A	127.7(6)
12	N2A	Ir1A	C13A	80.5(3)	47	C7A	C8A	C9A	118.0(7)
13	N3A	Ir1A	C8A	100.2(3)	48	C8A	C9A	H9A	120.0(8)
14	N3A	Ir1A	C13A	171.3(3)	49	C8A	C9A	C10A	120.1(8)
15	C8A	Ir1A	C13A	88.0(3)	50	H9A	C9A	C10A	119.9(9)
16	Ir1A	O1A	C30A	116.0(5)	51	F2A	C10A	C9A	119.5(8)
17	Ir1A	N1A	C1A	117.3(5)	52	F2A	C10A	C11A	117.4(8)
18	Ir1A	N1A	C5A	124.1(5)	53	C9A	C10A	C11A	123.1(9)
19	C1A	N1A	C5A	118.5(6)	54	C10A	C11A	H11A	121.4(9)
20	Ir1A	N2A	C19A	116.5(5)	55	C10A	C11A	C12A	117.1(8)
21	Ir1A	N2A	C23A	123.4(5)	56	H11A	C11A	C12A	121.5(8)
22	C19A	N2A	C23A	120.1(6)	57	F1A	C12A	C7A	119.5(6)
23	Ir1A	N3A	C25A	126.6(5)	58	F1A	C12A	C11A	117.4(7)
24	Ir1A	N3A	C29A	114.7(5)	59	C7A	C12A	C11A	123.1(7)
25	C25A	N3A	C29A	118.8(7)	60	Ir1A	C13A	C14A	127.0(5)
26	N1A	C1A	C2A	120.2(6)	61	Ir1A	C13A	C18A	113.5(5)
27	N1A	C1A	C7A	112.3(6)	62	C14A	C13A	C18A	119.5(7)
28	C2A	C1A	C7A	127.5(6)	63	C13A	C14A	H14A	120.6(8)
29	C1A	C2A	H2A	120.0(7)	64	C13A	C14A	C15A	118.8(7)
30	C1A	C2A	C3A	120.0(7)	65	H14A	C14A	C15A	120.6(8)
31	H2A	C2A	C3A	120.0(7)	66	F4A	C15A	C14A	117.8(7)
32	C2A	C3A	C4A	119.3(7)	67	F4A	C15A	C16A	117.9(7)
33	C2A	C3A	C6A	120.3(7)	68	C14A	C15A	C16A	124.3(8)
34	C4A	C3A	C6A	120.4(8)	69	C15A	C16A	H16A	122.5(9)
35	C3A	C4A	H4A	120.3(8)	70	C15A	C16A	C17A	114.9(8)

Number	Atom1	Atom2	Atom3	Angle(°)	Number	Atom1	Atom2	Atom3	Angle(°)
71	H16A	C16A	C17A	122.6(9)	92	C22A	C23A	H23A	118.9(8)
72	F3A	C17A	C16A	115.6(7)	93	O4A	C24A	C21A	121.3(9)
73	F3A	C17A	C18A	118.8(7)	94	N3A	C25A	H25A	119.0(8)
74	C16A	C17A	C18A	125.6(7)	95	N3A	C25A	C26A	121.9(8)
75	C13A	C18A	C17A	116.9(6)	96	H25A	C25A	C26A	119.0(9)
76	C13A	C18A	C19A	116.0(6)	97	C25A	C26A	H26A	120(1)
77	C17A	C18A	C19A	127.1(7)	98	C25A	C26A	C27A	119(1)
78	N2A	C19A	C18A	113.5(6)	99	H26A	C26A	C27A	120(1)
79	N2A	C19A	C20A	118.6(6)	100	C26A	C27A	H27A	121(1)
80	C18A	C19A	C20A	127.9(6)	101	C26A	C27A	C28A	119(1)
81	C19A	C20A	H20A	119.6(7)	102	H27A	C27A	C28A	121(1)
82	C19A	C20A	C21A	120.8(7)	103	C27A	C28A	H28A	120(1)
83	H20A	C20A	C21A	119.6(8)	104	C27A	C28A	C29A	119.6(9)
84	C20A	C21A	C22A	119.2(8)	105	H28A	C28A	C29A	120(1)
85	C20A	C21A	C24A	120.0(7)	106	N3A	C29A	C28A	121.3(8)
86	C22A	C21A	C24A	120.8(8)	107	N3A	C29A	C30A	115.5(7)
87	C21A	C22A	H22A	120.5(8)	108	C28A	C29A	C30A	123.2(7)
88	C21A	C22A	C23A	119.0(8)	109	O1A	C30A	O2A	123.7(8)
89	H22A	C22A	C23A	120.5(8)	110	O1A	C30A	C29A	117.1(7)
90	N2A	C23A	C22A	122.3(7)	111	O2A	C30A	C29A	119.2(7)
91	N2A	C23A	H23A	118.8(7)	112	Cl1	C3	Cl2	108.5(9)

Table S2. Complete list of bond lengths in IrC

Number	Atom1	Atom2	Length (Å)	Number	Atom1	Atom2	Length (Å)
1	Ir1A	O1A	2.155(7)	33	C9A	H9A	0.931(8)
2	Ir1A	N1A	2.017(5)	34	C9A	C10A	1.36(1)
3	Ir1A	N2A	2.037(6)	35	C10A	C11A	1.37(1)
4	Ir1A	N3A	2.141(6)	36	C11A	H11A	0.930(9)
5	Ir1A	C8A	1.997(9)	37	C11A	C12A	1.36(1)
6	Ir1A	C13A	2.009(6)	38	C13A	C14A	1.375(8)
7	F1A	C12A	1.370(8)	39	C13A	C18A	1.42(1)
8	F2A	C10A	1.33(1)	40	C14A	H14A	0.931(7)
9	F3A	C17A	1.367(9)	41	C14A	C15A	1.37(1)
10	F4A	C15A	1.373(8)	42	C15A	C16A	1.38(1)
11	O1A	C30A	1.27(1)	43	C16A	H16A	0.930(8)
12	O2A	C30A	1.23(1)	44	C16A	C17A	1.344(9)
13	O3A	C6A	1.19(1)	45	C17A	C18A	1.386(9)
14	O4A	C24A	1.20(1)	46	C18A	C19A	1.453(7)
15	N1A	C1A	1.370(9)	47	C19A	C20A	1.408(9)
16	N1A	C5A	1.36(1)	48	C20A	H20A	0.930(8)
17	N2A	C19A	1.355(9)	49	C20A	C21A	1.363(9)
18	N2A	C23A	1.346(8)	50	C21A	C22A	1.38(1)
19	N3A	C25A	1.34(1)	51	C21A	C24A	1.49(1)
20	N3A	C29A	1.34(1)	52	C22A	H22A	0.930(6)
21	C1A	C2A	1.390(9)	53	C22A	C23A	1.37(1)
22	C1A	C7A	1.46(1)	54	C23A	H23A	0.930(7)
23	C2A	H2A	0.931(8)	55	C25A	H25A	0.93(1)
24	C2A	C3A	1.38(1)	56	C25A	C26A	1.37(1)
25	C3A	C4A	1.37(1)	57	C26A	H26A	0.93(1)
26	C3A	C6A	1.49(1)	58	C26A	C27A	1.37(2)
27	C4A	H4A	0.930(9)	59	C27A	H27A	0.93(1)
28	C4A	C5A	1.365(9)	60	C27A	C28A	1.37(2)
29	C5A	H5A	0.930(8)	61	C28A	H28A	0.93(1)
30	C7A	C8A	1.418(9)	62	C28A	C29A	1.37(1)
31	C7A	C12A	1.39(1)	63	C29A	C30A	1.51(1)
32	C8A	C9A	1.39(1)	64	Cl3	C1	1.79(3)

Table S3. Intermolecular Hydrogen Bond Interactions for IrC

D-H···A	d(D-H) [Å]	d(H···A) [Å]	d(D···A) [Å]	<(DHA) [°]
C(2A)--H(2A)···F(1A)	0.93	2.24	2.853(9)	123
C(20A)--H(20A)···F(3A)	0.93	2.28	2.881(10)	122
C(4A)--H(4A)···O(2A) i	0.93	2.78	3.548(11)	141
C(5A)--H(5A)···O(1A)	0.93	2.57	3.148(9)	121
C(6A)--H(6A)···O(2A) i	0.93	2.48	3.286(12)	145
C(11A)--H(11A)···O(4A) ii	0.93	2.87	3.629(12)	140
C(20A)--H(20A)···O(1A) iii	0.93	2.87	3.601(9)	136
C(24A)--H(24A)···O(1A) iii	0.93	2.52	3.340(11)	147
C(25A)--H(25A)···O(3A) iv	0.93	2.41	3.211(13)	145
C(26A)--H(26A)···O(4A) v	0.93	2.89	3.753(15)	155
C(23A)--H(23A)···N(3A)	0.93	2.58	3.160(9)	121

Symmetry transformations used to generate equivalent atoms: i) 1-x,2-y,1-z; ii) 1-x,1-y,-z; iii)1-x,2-y,-z; iv) 1-x,1-y,1-z; v) 2-x,1-y,-z;

Table S4. Intermolecular C-X--π(Cg) interactions for IrC

C-X··· π(Cg)	d(X··· π(Cg) [Å]	<(CXCg) [°]
C(12A) -F(1A)···Cg(4) i	3.402(6)	100.2
C(17A) -F(3A)···Cg(5) ii	3.526(7)	88.6
C(6A) -O(3A)···Cg(7) i	3.667(11)	85.5
C(24A) -O(4A)···Cg(8) ii	3.657(8)	71.8

Cg: centroid of the π ring system; Cg(4) = N1A-C1A-C2A-C3A-C4A-C5A; Cg(5) = N2A-C19A-C20A-C21A-C22A-C23A; Cg(7) = C7A-C8A-C9A-C10A-C11A-C12A; Cg(8) = C13A-C14A-C15A-C16A-C17A-C18A. Symmetry transformations used to generate equivalent atoms: i) 1-x,1-y,1-z; ii) 1-x,2-y,-z.

Table S5. Calculated absorption of IrC and IrC+$(CN)_2$ in CH_3CN media at TD-B3LYP level together with experimental values

	State	λ(nm)/E(eV)	Oscillator	Main configuration	Assign	λ_{exp} (nm)
IrC	S_1	497/2.49	0.0220	H→L (90%)	Ir/dfppy → dfppy/CHO (MLCT/LLCT)/	475
	S_4	397/3.12	0.1524	H-1→L (71%)	Ir/ dfppy /pic → dfppy (MLCT/LLCT/ILCT)	340
	S_{14}	343/3.61	0.1406	H→L+3 (82%)	Ir/ dfppy → Ir/ dfppy /CHO/pic (MLCT/LLCT/ILCT)	340
	S_{16}	337/ 3.67	0.0893	H-5→L+1 (76%)	Ir/ dfppy /pic→ CHO (MLCT/ILCT)	340
	S_{18}	322/ 3.84	0.0138	H-1→L+2 (69%)	pic/Ir/dfppy → pic (MLCT/ILCT/LLCT)	
IrC+$(CN)_2$	S_1	406/3.05	0.0545	H→L (94%)	Ir/ dfppy → Ir (ILCT/ MLCT)	456
	S_2	393/3.15	0.0053	H→L+1(95%)	Ir/ dfppy → pic/Ir/ dfppy (ILCT/ MLCT/ LLCT)	375
	S_5	338/3.67	0.089	H-1→L+1 (74%)	pic/Ir/ dfppy → pic/Ir/ dfppy (ILCT/ MLCT/ LLCT)	
	S_7	328/3.77	0.0350	H-1→L+2 (63%)	pic/Ir/ dfppy → pic/Ir/ dfppy (MLCT/ LLCT/ ILCT)	
	S_{10}	318/ 3.90	0.0483	H→L+4 (33%)	Ir/ dfppy → pic (MLCT/ LLCT)	
	S_{12}	308/4.01	0.0094	H→L+5 (89%)	Ir/ dfppy → pic (MLCT/ LLCT)	312
	S_{13}	306/ 4.05	0.0911	H-2→L+2 (25%)	pic/Ir/ dfppy → pic/Ir (MLCT/ LLCT/ ILCT)	312
	S_{15}	302/ 4.10	0.1572	H-4→L (54%)	pic/Ir/ dfppy → Ir/ dfppy (MLCT/ LLCT/ ILCT)	312
	S_{20}	290/ 4.28	0.0278	H-5→L (47%)	pic/Ir/ dfppy → Ir/ dfppy (MLCT/ LLCT/ ILCT)	253

Table S6. Comparison of present manuscript with previous reports with respect to type of heavy metal complexes used for the detection of cyanide.

S. No.	Publication	System	Detection limit
1	Current work	Highly selective chemosensor for cyanide based on formyl functionalized phosphorescent iridium(III) complex	2.16×10^{-8} M (in acetonitrile) and ~264.8 ng/mL (in drinking water)
2	*New J. Chem. 2010, 34, 132–136*	Multisignaling detection of cyanide anions based on an iridium(III) complex: remarkable enhancement of sensitivity by coordination effect	40×10^{-6} (in drinking water)
3	*J. Am. Chem. Soc. 2011, 133, 15276–15279*	Iridium(III) complex-coated nanosystem for ratiometric upconversion luminescence bioimaging of cyanide anions	0.18×10^{-6} M
4	*Adv. Funct. Mater.* 2012, *22*, 2667–2672	Iridium-complex-modified upconversion nanophosphors for effective lret detection of cyanide anions in pure water	62.6×10^{-6} M
5	*Chem. Commun.,* 2013, 49, 255-257	A CN^- specific turn-on phosphorescent probe with probable application for enzymatic assay and as an imaging reagent	0.38×10^{-6} M (in buffer medium of pH 7.6.)
6	*Chem. Commun.,* 2012, 48, 2707–2709	A lab-on-a-molecule for anions in aqueous solution: using Kolbe electrolysis and radical methylation at iridium for sensing	-
7	*Microchim Acta, 2015 182, 2561–2566*	Silica nanoparticles doped with an iridium(III) complex for rapid and fluorometric detection of cyanide	1.66×10^{-6} M
8	*Inorg. Chem. 2013, 52, 4890−4897*	Switching of reverse charge transfers for a rational design of an OFF−ON phosphorescent chemodosimeter of cyanide anions	6×10^{-6} M
9	*Inorg. Chem. 2012, 51, 7075−7086*	Rapid and highly sensitive dual-channel detection of cyanide by bis-heteroleptic ruthenium(II) complexes	0.18×10^{-6} M
10	*Dalton Trans., 2015, 44, 18607-18623*	Pyrene and imidazole functionalized luminescent bimetallic Ru(II) terpyridine complexes as efficient optical chemosensors for cyanide in aqueous, organic and solid media	9.79×10^{-8} M

Table S7. Optimized geometries, HOMO and LUMO contour plots of the metal complexes at the B3LYP/6-31G* level

	IrC	IrC+$(CN)_2$
Optimized geometries at the B3LYP/6-31G* level	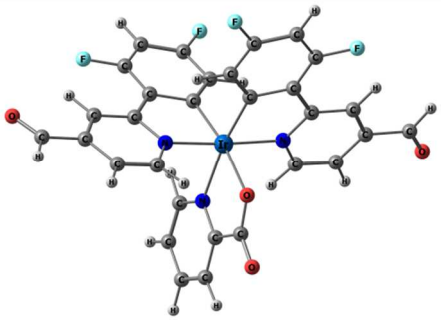	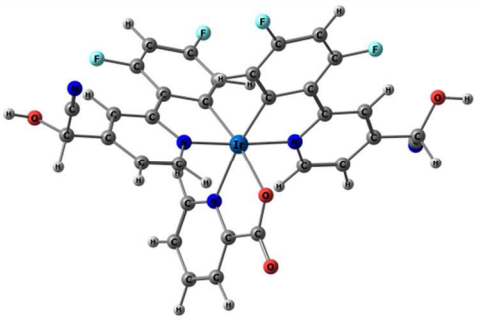
LUMO+3	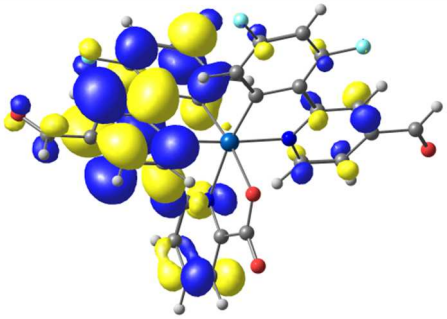	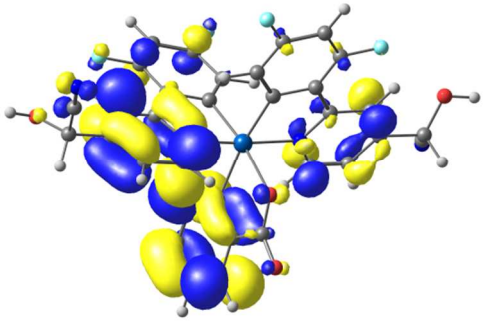
LUMO+2	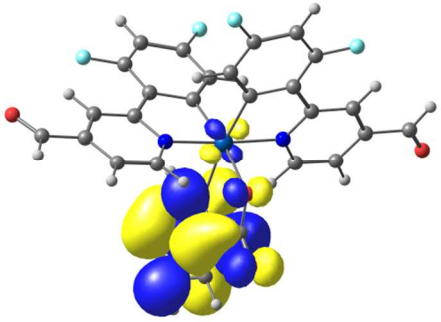	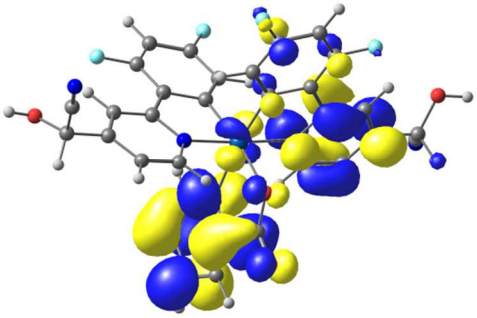
LUMO+1	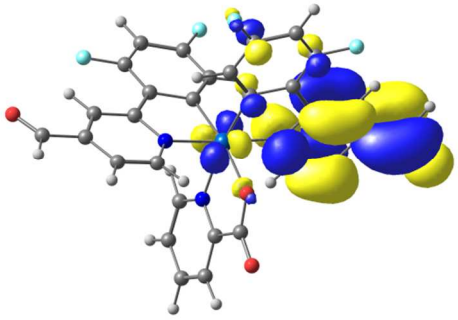	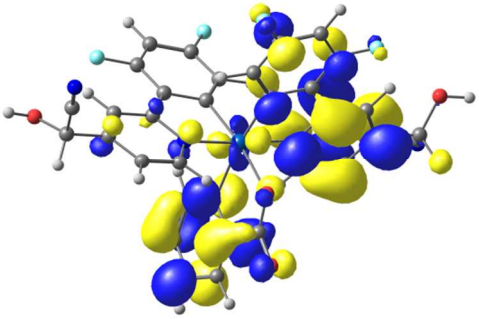

LUMO	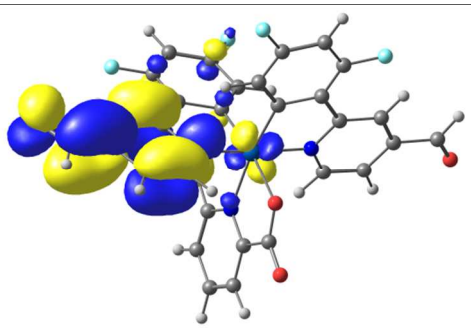	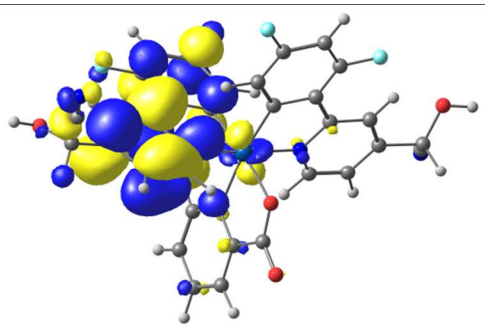
HOMO	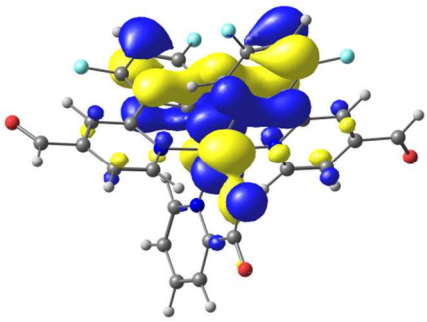	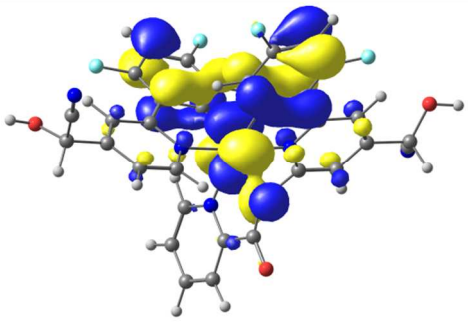
HOMO-1	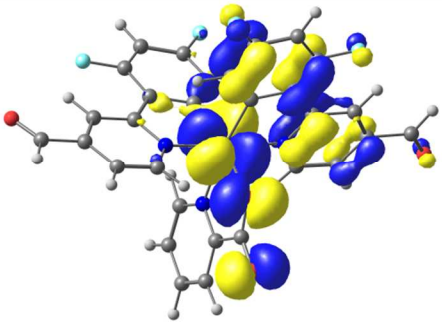	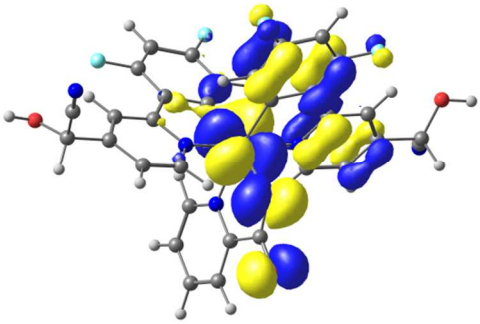
HOMO-2	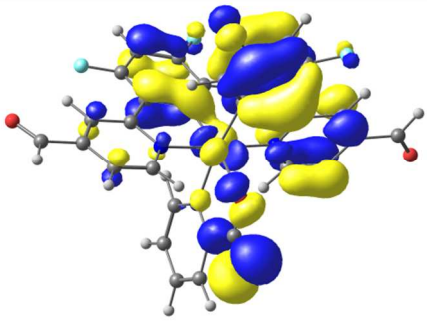	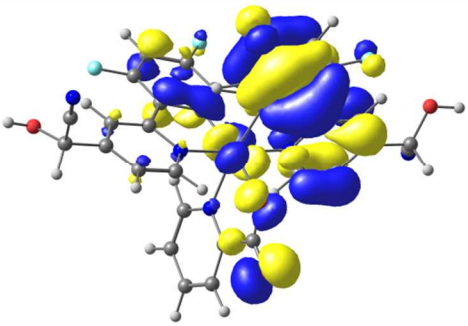
HOMO-3	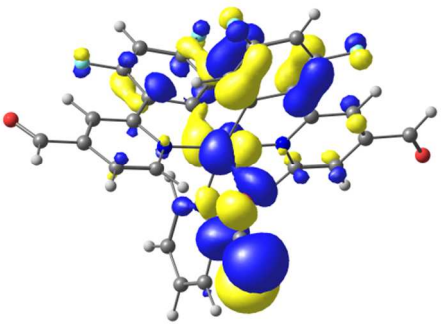	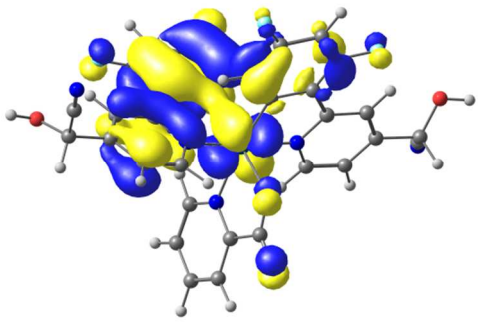

1. Cyclic voltammetry:

Results and discussion. To realize the electronic effects caused by the change of substituents on the C4′ position on the pyridyl moiety of the cyclometalated ligand in **IrC**, the electrochemical behaviour of **IrC** has been studied before and after the addition of 2.0 equivalents of CN^- anions by cyclic voltammetry experiments in deaerated CH_3CN solution using ferrocene as the internal standard and the results are depicted in Figure S21. The calculated HOMO and LUMO for **IrC** and its cyanide adduct are listed in Table S8. Quasi-reversible oxidation voltammograms were observed at identical potentials (~1.46 to 1.47 V) for both experiments (before and after the addition of CN^- anions), indicating the oxidation potential originated from the iridium metal center (Ir^{3+}/Ir^{4+}) has been least affected by the change of substituent from –CHO to −CH(CN)OH (cyanohydrin). Correspondingly, the calculated energy levels of highest occupied molecular orbitals (HOMO) stands almost same (–5.82 eV) in both cases. While scanning to the negative potential range, **IrC** exhibits two irreversible reduction potentials. First reduction potential occurs at −0.94 V can be attributed to the reduction of the –CHO group as usually found in formyl group substituted iridium(III) complexes and aromatic aldehydes.[1] Second reduction potential occurs at −1.70 V could be due to the reduction of N-coordinating pyridyl moiety of the cyclometalated ligand. Upon addition of 2.0 equiv of the CN^- ions to the experimental solution, the reduction potential correspond to –CHO substituent observed at −0.94 has been completely vanished and the cyclometalated ligand based reduction peak at −1.63 V dominates. The calculated LUMO experienced a more positive shift (~0.71 eV) from −3.43 to −2.72 eV. This observation clearly points out the change in the localization of LUMO from –CHO group to cyclometalated ligand upon conversion of –CHO substituent to –CH(CN)OH (cyanohydrin).

These assumptions were strongly supported by the density functional theory (DFT) calculations (see main article).

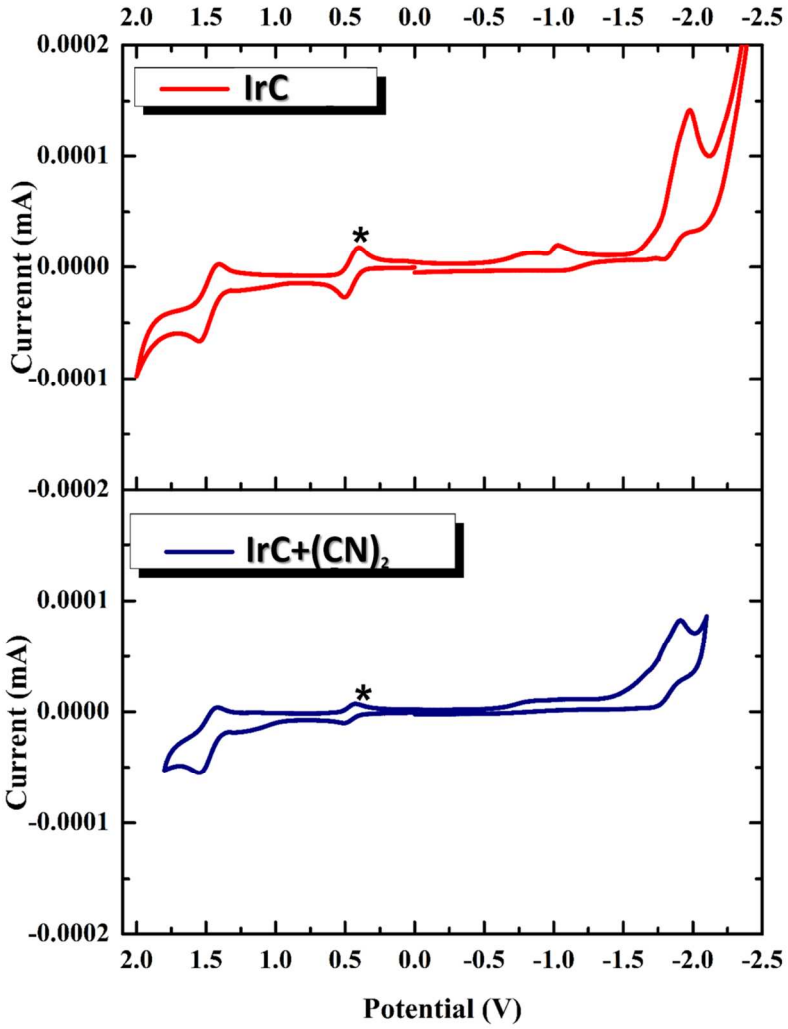

Figure S21. Comparison of redox potentials (vs Ag/AgCl in CH_3CN) of **IrC** before and after the addition of 2.0 equiv of CN^-, (oxidation potential $FeCp_2/FeCp_2^+$ =0.44 V, marked with asterisk).

Table S8. Electochemical properties of IrC and IrC+$(CN)_2$

Complex	E_{oxd} [a](V)	E_{red} [a] (V)	HOMO[b] (eV)	LUMO[c] (eV)	$E_{g(elec)}$ [d] (eV)	$E_{g(calc)}$ [e] (eV)
IrC	1.46	-0.94	-5.82	-3.43	2.39	3.01
		-1.70				
IrC+$(CN)_2$	1.47	-1.63	-5.83	-2.72	3.11	3.62

[a]Electrochemical data versus ($FeCp_2^+/FeCp_2^0$) ($FeCp_2$ is ferrocene) were collected in CH_3CN/0.1 M TBAH (tetra-butylammoniumhexafluorophosphate). [b]HOMO = -[4.8-(0.44) + E_{oxd}]. [c]LUMO = -[4.8 -(0.44) + E_{red}]. [d]Electrochemical band gap experimental. [e]Electrochemical band gap theoretical.

REFERENCES

(1) (a) Bejoymohandas, K. S.; Kumar, A.; Varughese, S.; Varathan, E.; Subramanian, V.; Reddy, M. L. P., *J. Mater. Chem. C* **2015,** *3*, 7405-7420. (b) Udhayan, R.; Basheerahmed, K.; Srinivasan, K., *Bull. Electrochem.* **1988,** *4*, 163-165.